RSC Advances

ROYAL SOCIETY OF CHEMISTRY

www.rsc.org/advances

Journal Name

ARTICLE

Core-shell $BaYbF_5$:Tm@$BaGdF_5$:Yb,Tm nanocrystals for *in vivo* tri-modal UCL/CT/MR imaging

Received 00th January 20xx,

Accepted 00th January 20xx

DOI: 10.1039/x0xx00000x

www.rsc.org/

Peng Zhang,[a] Yangyang He,[b] Jianhua Liu,[a] Jing Feng,[c] Zhiqiang Sun,[d] Pengpeng Lei,[c] Qinghai Yuan*[a] and Hongjie Zhang[c]

The lanthanide-doped nanocrystals have been researched extensively and used for bioimaging because of optical properties, magnetic properties and X-ray absorption. The core-shell structured lanthanide-doped nanocrystals have been developed and characterized by TEM and XRD analysis. The nanocrystals are composed of $BaYbF_5$:0.5%Tm as the core and $BaGdF_5$:20%Yb, 0.5%Tm as the shell. Apart from characterization of nanocrystals, evaluation of both cytotoxicity by MTT assays and long-term toxicity by histological analysis showed their low cytotoxicity, indicating the possibility for further *in vivo* imaging. This work combined the functions of tri-model imaging into one nanoplatform, and then the UCL, CT, and MR imaging of core-shell structured nanocrystals were investigated both *in vitro* and *in vivo*. Taking into consideration of the structural characteristics and tri-modal imaging abilities, it is expected that the developed multifunctional nanoplatform may be potentially useful for diagnosing diseases at an early stage.

Introduction

In the past twenty years, the lanthanide-doped nanocrystals have been researched extensively because of optical properties, such as long luminescence lifetime (μs-ms range), large Stokes (up to 500 nm), sharp emission bandwidths (<10 nm), these nanocrystals have been successfully applied in laser source, biological labeling and so on.[1-6] Besides, the lanthanide-doped nanocrystals have attracted much interest in diagnostics because of X-ray absorption and magnetic properties.[7-12] Recently, lanthanide-doped nanoprobe is a fascinating area especially for the multi-modal imaging.[12-18]

Many imaging techniques have been used for disease diagnosis, such as, ultrasound imaging, magnetic resonance imaging (MRI), computed tomography (CT), positron emission tomography (PET), and so on.[19-23] Among these imaging modalities, CT imaging has been recognized as one of the most useful imaging modalities because of the high spatial resolution, deep tissue penetration and powerful post-processing techniques, such as 3D volume rendering technique. Nanoprobe composed of lanthanide-doped elements with atomic number (Z ＞50) usually present excellent effect during CT imaging.[24-27] In spite of the advantages of the CT, this imaging technique is not sensitive for diagnosing diseases of soft tissue. However, MR imaging has advantages for examining soft tissue in musculoskeletal system or brain diseases. MRI has been widely used in diagnosis of diseases because of its admirable soft-tissue contrast and deep tissue penetration. For early or differential diagnosis of diseases, contrast materials are usually required. Recently, lanthanide-doped nanocrystals have generated a great deal of interest for CT or MR imaging.[28-37] Although CT and MR imaging has above advantages, these two techniques own the similar shortage: the resolution of CT and MR is about 50 μm and 10-100 μm, respectively.[38] The resolution is unable of cellular imaging. Optical imaging, on the other hand, has high resolution and sensitivity for imaging at the cellular level, such as the resolution of fluorescence reflectance imaging is about 2-3 mm.[38] The above problems arouse high attention of researchers in synthesis of lanthanide-doped nanocrystals for fluorescence imaging.[39-43] However, the optical imaging could not provide deep tissue penetration and 3D information. Therefore, multimodal imaging is attracting a great deal of attention, because it can integrate the merits of different techniques and improve the efficiency of diagnosis.

With this in mind, we report the synthesis of multi-functional lanthanide-doped nanocrystals that are composed of $BaYbF_5$:0.5%Tm (hereinafter abbreviated as $BaYbF_5$:Tm) as the core and $BaGdF_5$:20%Yb,0.5%Tm (hereinafter abbreviated as $BaGdF_5$:Yb,Tm) as the shell. The core-shell structure was characterized by powder X-ray diffraction (XRD), transmission electron microscopy (TEM), and so on. The cytotoxicity and

[a] Department of Radiology, the Second Hospital of Jilin University, Changchun, 130041 (P. R. China). E-mail: yuanqinghai123@sina.com.
[b] Department of Pathology, the Second Hospital of Jilin University, Changchun, 130041 (P. R. China).
[c] State Key Laboratory of Rare Earth Resource Utilization, Changchun Institute of Applied Chemistry, Chinese Academy of Sciences,Changchun, 130022 (P. R. China)
[d] Department of Interventional Therapy, Cancer Hospital of Jilin Province, Changchun, 132000 (P. R. China).
† Electronic Supplementary Information (ESI) available: [details of any supplementary information available should be included here]. See DOI: 10.1039/x0xx00000x

tissue toxicity of the nanocrystals was described in details. Finally, this work combined the functions of tri-model imaging into one nanoplatform, and then the UCL, CT, and MR imaging of core-shell structured nanocrystals were investigated both *in vitro* and *in vivo*.

2. Materials and methods

2.1 Chemicals

Analytical grade $Ba(OH)_2 \cdot 8H_2O$ was purchased from Sinopharm Chemical Reagent Co. Ltd (Shanghai, China). Yb_2O_3 (99.9%), Gd_2O_3 (99.99%) and Tm_2O_3 (99.99%) were obtained from Aladdin Reagents (Shanghai, China). Oleic acid (OA, >90%), 1-octadecene (ODE, >90%), and CF_3COOH were purchased from Sigma-Aldrich. Other chemicals were of analytical grade and used as received without further purification.

2.2 Preparation of $BaYbF_5$: Tm nanocrystals

2 mmol $Ba(OH)_2$ was dissolved into 2 mL deionized water under vigorous magnetic stirring, HCF_3COO was added into above mixture at room temperature, and the solution was heated to 100 ℃ after PH of 7, and then dried in a vacuum drying oven at 60 ℃ for 24 h. The $Tm(CF_3COO)_2$ and $Yb(CF_3COO)_3$ were also prepared by the above procedure.

For the synthesis of $BaYbF_5$:Tm nanocrystals, 1 mmol $Ba(CF_3COO)_2$, 0.98 mmol $Yb(CF_3COO)_3$ and 0.02 mmol $Tm(CF_3COO)_3$ were added to 100 mL three-neck round-bottom, and then 10mL oleic acid and 10 mL octadecene were added, the mixture was heated to 100 ℃ with magnetic stirring for 0.5 h under an argon protective atmosphere, and then was heated to 300 ℃ for 1 h. After reacting completely, the system was naturally cooled down to room temperature. The prepared nanocrystals were isolated by centrifugation, washed with ethanol for several times, and then re-dispersed in cyclohexane. .

2.3 Synthesis of $BaYbF_5$:Tm@$BaGdF_5$:Yb,Tm nanocrystals

1 mmol $Ba(CF_3COO)_2$, 0.78 mmol $Gd(CF_3COO)_3$, 0.2 mmol $Yb(CF_3COO)_3$, 0.02 mmol $Tm(CF_3COO)_3$ were added to 100 mL three-neck round-bottom, and then 10 mL oleic acid and 10 mL octadecene mixed 1 mmol $BaYbF_5$:Tm were added, the mixture was heated to 100 ℃ with magnetic stirring for 0.5 h under an argon protective atmosphere, and then was heated to 300 ℃ for 1 h. After reacting completely, the system was naturally cooled down to room temperature. The prepared nanocrystals were isolated by centrifugation, washed with ethanol for several times, and then re-dispersed in cyclohexane.

2.4 Surface modification of $BaYbF_5$:Tm@$BaGdF_5$:Yb,Tm

$BaYbF_5$:Tm@$BaGdF_5$:Yb,Tm nanocrystals in chloroform (10 mL, 5 mg/mL) were mixed with chloroform solution of DSPE-PEG2000 (20 mL, 10 mg/mL) under stirring at room temperature for 10 minutes. The mixture was evaporated and the resultant solution was heated to 60 ℃ for 1 h under vacuum. After cooling, 10 mL deionized water was added. The solution was dispersed with ultrasound and then centrifuged at 10,000 rpm/min for 20 minutes. The PEG-modified nanocrystals were redispersed into deionized water for future use.

2.5 Measurements and Characterizations

The morphology and composition of the $BaYbF_5$:Tm@$BaGdF_5$:Yb,Tm nanocrystals were determined by a field emission scanning electron microscope (FESEM, S4800, Hitachi). The concentrations of nanocrystals were obtained by inductively coupled plasma-mass spectrometry (ICP-MS). X-ray powder diffraction (XRD) patterns were measured on a D8 ADVANCE (Germany) using Cu Kα (0.15406 nm) radiation. Transmission electron microscope (TEM) measurements were analyzed on a JEOL JEM-2010EX TEM.X-ray photoelectron (XPS) measurements were collected on an ESCALAB-MKII spectrometer (VG Co., United Kingdom). The UCL spectra were recorded by using a 980 nm laser diode and a triple grating monochromator (Spectra Pro-2758, Acton Research Corporation, USA) equipped with a photomultiplier (Hamamatsu R928). MRI images were obtained through a 1.5 T scanner (Achieva, Siemens, Germany).CT images were acquired using a 256-slice multidetector CT scanner (Brilliance iCT, Philips Healthcare, Cleaveland, Ohio, USA). MR images were obtained using 1.5T Achieva scanner (Siemens).

2.6 *In vitro* cytotoxicity studies

HepG2 cells were cultured in Dulbecco's modified Eagle's medium (DMEM) supplemented with 10% fetal bovine serum (FBS) and 1% penicillin-streptomycin in a humidified incubator at 37 ℃ under 5% CO_2. The HepG2 Cells were cultured and were again put back into fresh complete medium before plating.

The *in vitro* cytotoxicity of nanocrystals was evaluated by the HepG2 cell viability and proliferation through methyl thiazolyl tetrazolium (MTT) reduction assays. In a typical procedure, HepG2 cells were seeded into 96-well plates for 12 h to allow the cells to attach. Subsequently, DMEM mixture containing $BaYbF_5$:Tm@$BaGdF_5$:Yb,Tm-PEG nanocrystals with different concentrations (from 0-500 μg/mL) was added to the wells. The HepG2 cells were incubated in the incubator for another 24 h and washed with medium twice. Thereafter, MTT (10 μL, 5 mg/mL) was added to the samples for another 4 h, and then dimethyl sulfoxide (DMSO) was added into the wells to dissolve the formazan crystals. Finally, an enzyme-linked immunosorbent assay reader was applied to measure the absorbance at a wavelength of 570 nm.

2.7 Animal protocol and histopathology analysis

Kunming mice were obtained from Laboratory Animal Center of Jilin University (Changchun, China). Animal care and handing procedures were in agreement with the guidelines of the Institutional Animal Care and Use Committee.

Kunming mice with and without injection of $BaYbF_5$:Tm@$BaGdF_5$:Yb,Tm-PEG were sacrificed after 30 days. The tissues (kidney, heart, liver, spleen, lungs) were collected from above two groups, and then fixed in 10% neutral buffered formalin. Then, the well-prepared tissues were embedded in paraffin, and then sectioned in 4 μm thick, stained

with hematoxylin and eosin (H&E). The histological sections were analysed using an optical microscope.

2.8 UCL imaging

To evaluate upconversion luminescence imaging, chloral hydrate (10 wt%) was injected into the mouse intraperitoneally, and then 200 μL of $BaYbF_5$:Tm@$BaGdF_5$:Yb,Tm-PEG aqueous solution with the concentration of 10 mg mL^{-1} was injected into the mouse subcutaneously. After administration, the upconversion luminescence imaging was carried out through the *in vivo* Maestro whole-body imaging system equipped with an external 980 nm laser as the excitation source. The upconversion luminescence imaging was obtained with the exposure time of 5 s.

2.9 CT imaging

For *in vitro* CT imaging, $BaYbF_5$:Tm@$BaGdF_5$:Yb,Tm-PEG nanocrystals were dispersed in deionized water with different concentrations (0-236 mM). The Eppendorf tubes with different concentration of the nanocrystals and iobitridol were scanned using a Philips CT imaging system.

For *in vivo* CT imaging, after anesthetizing by intraperitoneal injection of 10 wt% chloral hydrate, mice were intravenously injected with $BaYbF_5$:Tm@$BaGdF_5$:Yb,Tm-PEG nanocrystals (20 mM mL^{-1}) and iobitridol (20 mM mL^{-1}), respectively.

CT images were obtainedfrom a Philips iCT Scanner. The scanning parameters included 120 kVp (tube voltage), 300 mA (tube current), 0.9 mm (thickness). Post process techniques of multiplanar-reconstruction (MPR) and volume rendering (VR) were used to get coronal images.

2.10 MR imaging

For *in vitro* MR imaging, nanocrystals were dispersed in deionized water with different concentrations (0-2.4 μM mL^{-1}). The Eppendorf tubes with different concentrations of nanocrystals and Gadolinium DTPA (Gd-DTPA) were scanned using a clinical MRI instrument for T1-weighted imaging (T_1WI).

For *in vivo* MR imaging, after anesthetizing by intraperitoneal injection of 10 wt% chloral hydrate, Kunming mice were subcutaneous injected with nanocrystals (20 mM mL^{-1}).

MR images were obtained from 1.5 T Achieva scanner (Siemens). The scanning parameters (T_1WI) included TR （time of repetition） =450, TE （time of echo） =14, Post process techniques of multi-planar-reconstruction (MPR) and volume rendering (VR) were used to get coronal images.

3. Results and discussion

3.1 Characterization of $BaYbF_5$:Tm@$BaGdF_5$:Yb,Tm nanocrystals

OA-stabilized $BaYbF_5$:Tm nanocrystals were synthesized using a high-temperature solvent thermal method. As shown in the transmission electron microscopy (TEM) image, these nanocrystals were regular quadrate with a mean diameter of 6 nm (Fig. 1a). TEM image of $BaYbF_5$:Tm@$BaGdF_5$:Yb,Tm nanocrystals demonstrated quadrate with a narrow size distribution and an average diameter of 9 nm (Fig. 1b). High-resolution TEM images clearly showed lattice fringes with an observed d-spacing of 0.29 nm, which was well consistent with the lattice spacing in the (010) planes of $BaYbF_5$:Tm (Fig. 1a, inset). X-ray diffraction (XRD) analysis further illustrated crystalline structure in Fig. 2. All the diffraction peaks could be well indexed to pure cubic phase $BaGdF_5$ (JCPDS No. 24-0098) very well, and no trace of other phases and impurities could be observed. The successful modification of PEG on the surface of $BaYbF_5$:Tm@$BaGdF_5$:Yb,Tm nanocrystals was confirmed by FTIR spectroscopy (Fig. 3). Two new bands at 1737 and 1109 cm^{-1} in the FTIR spectrum of PEG-UCNPs were assigned to the stretching vibration of the carboxyl ester and the ether bond of PEG chains, respectively. Fig. 4 demonstrated the UCL spectra of $BaYbF_5$:Tm (core) and $BaYbF_5$:Tm@$BaGdF_5$:Yb,Tm (core-shell) nanocrystals. $BaYbF_5$:Tm nanocrystals showed no obvious emission in the visible region and one mild emission in the NIR region. However, compared with core nanocrystals, the core-shell nanocrystals exhibited two emission s in the visible region and one obvious emission in the NIR region, upon excitation by a 980 nm laser. $BaYbF_5$:Tm@$BaGdF_5$:Yb,Tm nanocrystals show excellent NIR upconversion luminescence, whose intensity was very strong and more than five times the intensity of 475 nm UCL.

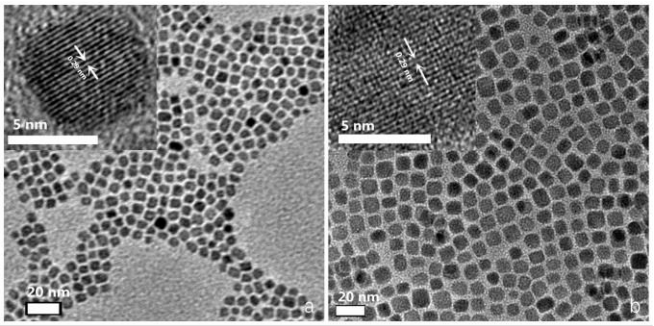

Fig. 1 a) TEM image of $BaYbF_5$:Tm nanocrystals. The inset shows a HRTEM image with a spacing of about 0.29 nm. b) TEM image of $BaYbF_5$:Tm@$BaGdF_5$:Yb,Tm. The inset shows a HRTEM image with a spacing of about 0.29 nm.

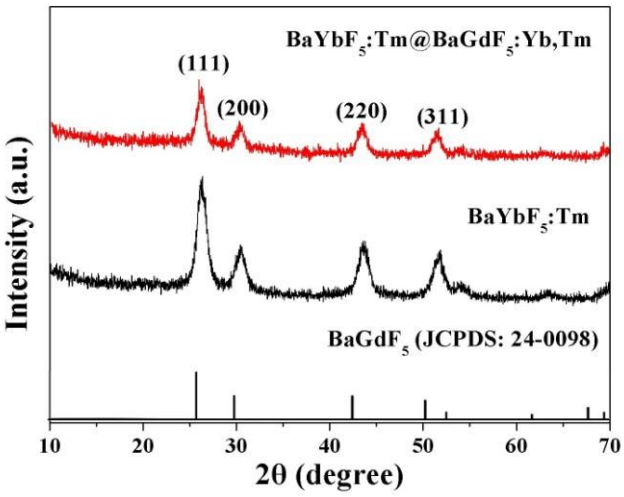

Fig. 2 XRD patterns of $BaYbF_5$:Tm and $BaYbF_5$:Tm@$BaGdF_5$:Yb,Tm nanocrystals. The line spectrum corresponds to the standard data of $BaGdF_5$ (JCPDS No. 24-0098).

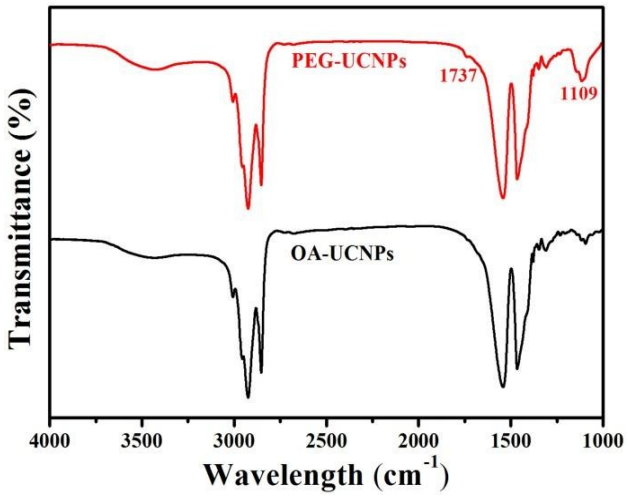

Fig. 3 FTIR spectra of OA-stabilized $BaYbF_5$:Tm@$BaGdF_5$:Yb,Tm and $BaYbF_5$:Tm@$BaGdF_5$:Yb,Tm-PEG nanocrystals.

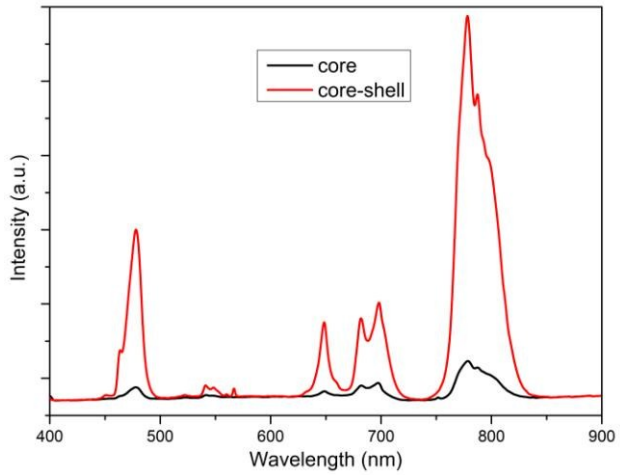

Fig. 4 UCL spectra of $BaYbF_5$:Tm (core) and $BaYbF_5$:Tm@$BaGdF_5$:Yb,Tm (core-shell) nanocrystals dissolved in water excited with a 980 nm laser, the power of 980 nm laser is 800 mw/cm^2.

3.2 Toxicology investigation

Encouraged by the high efficient NIR upconversion luminescence imaging, the *in vitro* and *in vivo* toxicity of $BaYbF_5$:Tm@$BaGdF_5$:Yb,Tm-PEG nanocrystals were carried out. The *in vitro* cytotoxicity was evaluated on HepG2 cells through MTT assay, and the *in vivo* cytotoxicity was evaluated on histological changes of several tissues after injection nanocrystals of one month.

MTT assay results were illustrated in Fig. 5, the viability of HepG2 cells treated with $BaYbF_5$:Tm@$BaGdF_5$:Yb,Tm-PEG nanocrystals still remained approximately 90% even at the highest tested dose (500 μg/mL). No significant differences in the proliferation of the cells were observed in the presence of 0-500μg/ml.

Results of histopathology analysis were shown in Fig. 6. The tissues from kidney, heart, liver, spleen and lungs were normal in the control group which was not injected nanocrystals. Compared with control group, no tissue damage or any other side effect from mice injected with $BaYbF_5$:Tm@$BaGdF_5$:Yb,Tm-PEG nanocrystals.

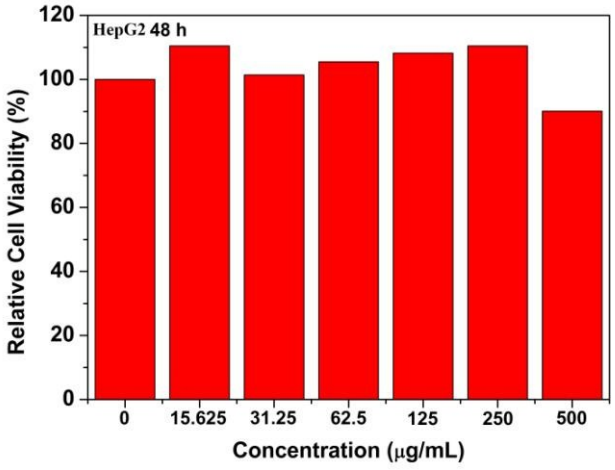

Fig. 5 *In vitro* cell viability of HepG2 cells incubated with $BaYbF_5$:Tm@$BaGdF_5$:Yb,Tm-PEG nanocrystals at different concentration.

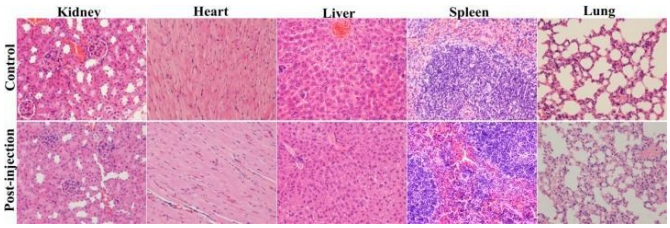

Fig. 6 Histological changes in the control group and imaging group. Hematoxylin and eosin (H&E) stained histological image of tissue of kidney, heart, liver, spleen and lungs with or without nanocrystals injection at 400× magnification.

3.3 UCL imaging

Since $BaYbF_5$:Tm@$BaGdF_5$:Yb,Tm-PEG nanocrystals had obvious emissions both in the visible region and in the NIR region. We investigated the feasibility for *in vivo* UCL imaging of the nanocrystals (980 nm, 0.8 w/cm^2). Fig. 7 shows the *in vivo* imaging of mice with subcutaneous injection of the $BaYbF_5$:Tm@$BaGdF_5$:Yb,Tm-PEG nanocrystals. As shown in Fig. 6, an intense UC signal was observed after the injection (Fig. 7a), while there were no signals in white light imaging (Fig. 7a). The overlay image showed an excellent matching of white light and UC emission bioimaging. This result indicated that the nanocrystals were perfect for *in vivo* UCL bioimaging.

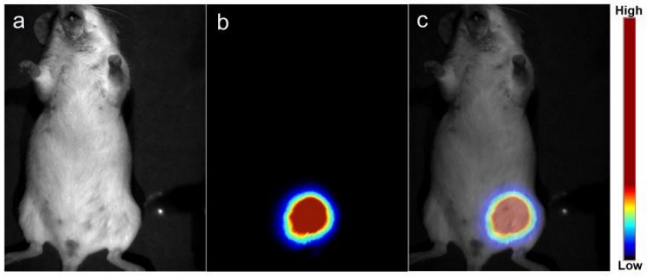

Fig.7 *In vivo* upconversion luminescence imaging of the mouse with injection of $BaYbF_5$:Tm@$BaGdF_5$:Yb,Tm-PEG nanocrystals: the left panel is white light imaging (a), the middle panel is UC emission imaging (b), right panel is overlay image (c). The wavelength collected for small animal imaging is from 795 nm to 805 nm.

3.4 Computed tomography imaging

Our previous study showed that the bimetallic nanomaterials composed of high atomic number showed excellent CT imaging effect.[39-42] Compared with iobitridol (iodine) (53), $BaYbF_5$:Tm@$BaGdF_5$:Yb,Tm-PEG nanocrystals had Ba (56), Yb (70), Gd (64), and Tm (69) elements, and my hold a great promise as a novel CT contrast agents.

To evaluate the feasibility and efficiency of the $BaYbF_5$:Tm@$BaGdF_5$:Yb,Tm-PEG nanocrystals, *in vitro* CT imaging was performed by scanning the Eppendorf tubes containing nanocrystals with different concentration (0-236 mM). The effect of X-ray absorption was calculated by measuring CT attenuation value of nanocrystals in Hounsfield Unit (HU). As shown in Fig. 8, the nanocrystals demonstrated an excellent X-ray absorption comparing to iobitridol, which was clinically used for many years (Fig. 8a-b). The CT attenuation value (HU) was increased accompany with improve concentration of nanocrystals (Fig. 8c), and the linear correlation between them was good. Furthermore, the absorption efficiency of nanocrystals was higher than that of iobitridol at the same molar concentration. Based on above results, $BaYbF_5$:Tm@$BaGdF_5$:Yb,Tm-PEG nanocrystals provided higher absorption efficiency than that of element I.

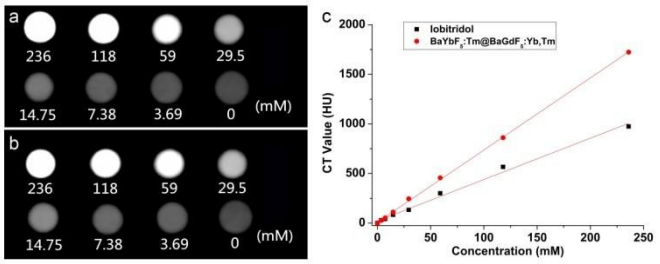

Fig. 8 a) CT images of $BaYbF_5$:Tm@$BaGdF_5$:Yb,Tm-PEG nanocrystals with different concentrations. b) X-ray CT images of iobitridol with different concentrations. c) CT value (HU) of different concentrations between nanocrystals (red) and iobitridol (black), respectively.

For *in vivo* CT imaging, the Kunming mice were scanning using iCT several times before and after injection of nanocrystals and iobitridol, respectively. The scanning times were pre-injection, 3 min, 30 min, 1 h and 2 h after injection. After admistration nanocrystals, 3 min later, the liver (Fig. 9 row a) and spleen (Fig. 9 row b) were enhanced, and the enhancement were increased gradually, and there were no enhancement after 2 h injection, the phenomenon was easily recognized using volume rendering technique (Fig. 9 row c). Compared with nanocrystals, iobitridol was discharged from urinary system (Fig. 10). After admistration iobitridol, 3 min later, the kidney were enhanced (Fig. 10 row b), and the bladder was showed after 30 min, the liver and spleen were not enhanced after 3 min. The detection of hepatic metastases may be improved from long-lasting liver-signal enhancement.

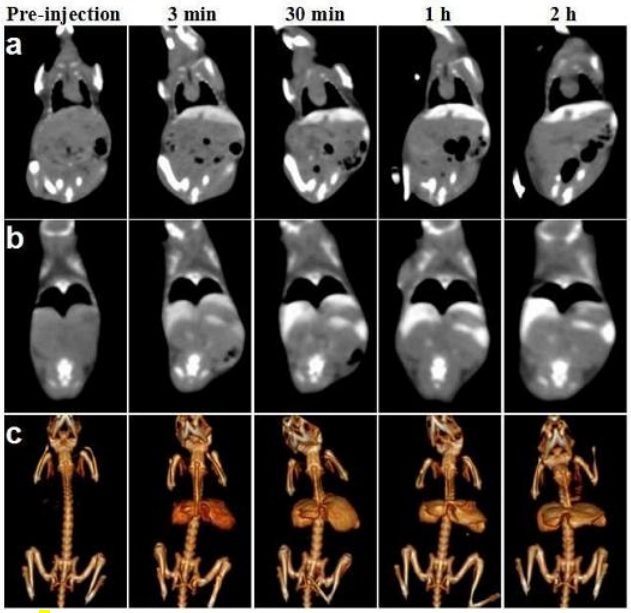

Fig. 9 CT images of mice after intravenous injection 1mL $BaYbF_5$:Tm@$BaGdF_5$:Yb,Tm-PEG nanocrystals (118 mM mL^{-1}) solution at timed intervals. (a) Liver. (b) Spleen and kidney. (c) Volume rendering technique of CT images.

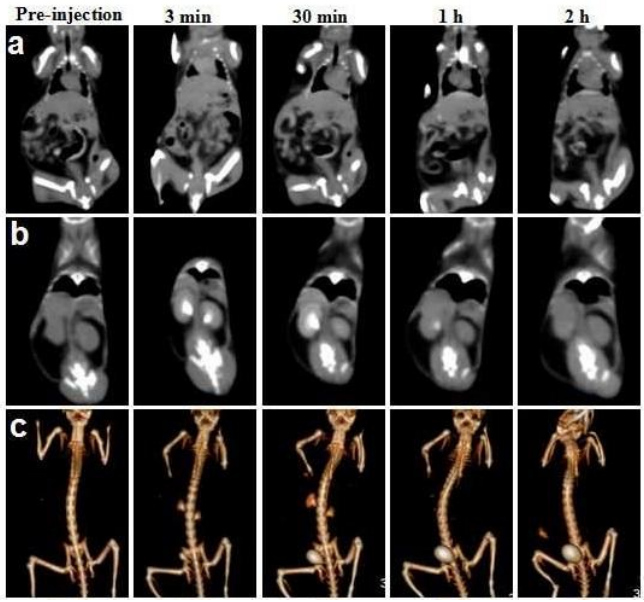

Fig. 10 CT images of mice after intravenous injection 1 mL iobitridol (118 mM mL^{-1}) solution at timed intervals. (a) Liver. (b) Spleen and kidney. (c) Volume rendering technique of CT images.

3.5 MR imaging

The Gd (III) ions existed in $BaYbF_5$:Tm@$BaGdF_5$:Yb,Tm-PEG nanocrystals enabled enhancement T_1MR imaging of mice. *In vitro* MR imaging was performed by scanning the Eppendorf tubes containing nanocrystals with different concentration (0-2.4 μM/mL). As shown in Fig. 11a-b, the MR signal demonstrated similar effect comparing to Gd- DTPA. For *in vivo* T_1WI MR imaging, the Kunming mice were scanning using 1.5 T clinical Scanner. Fig. 11c showed the muscle signal without injection (arrow), and Fig. 11d showed oval high signal after subcutaneous injection of nanocrystals (arrow).

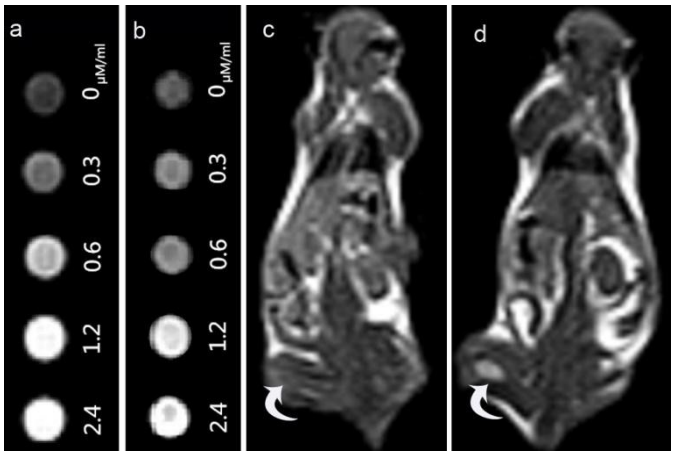

Fig. 11 a) T_1WI MR images of Gd- DTPA with different concentrations. b) T_1WI MR images of $BaYbF_5$:Tm@$BaGdF_5$:Yb,Tm-PEG nanocrystals with different concentrations. c) MR images showed muscle signal before injection nanocrystals (arrow). d) MR images showed high signal after injection nanocrystals (arrow).

4. Conclusions

In conclusion, $BaYbF_5$:Tm@$BaGdF_5$:Yb,Tm-PEG core-shell structured nanocrystals have been successfully constructed. The nanocrystals show monosized distributionand sub-10 nm diameter. Apart from characterization of nanocrystals, evaluation of both cytotoxicity by MTT assays and long-term toxicity by histological analysis showed their low cytotoxicity, indicating the possibility for further *in vivo* imaging. This multifunctional nanocrystals has been used as nanoplatform for upconversion luminescent, computed tomography and magnetic resonance tri-modal imaging of some major organs of mice. The Gd (III) ions enable enhancement in T1MR imaging, the shell of $BaGdF_5$:Yb,Tm shows perfect UCL emission and enhancement in CT imaging. Taking into consideration of the structural characteristics and tri-modal imaging abilities, it is expected that the developed multifunctional nanoplatform may be especially for diagnosing diseases on early stage.

Acknowledgements

Financial supports were provided by Technology Development Project of National Development and Reform Commission of Jilin province (No.JF2012c007-1).

Notes and references

1 F. Wang and X. Liu, *Chem Soc Rev*, 2009, **38**, 976-989.
2 S. Zhang, Y. Yao, X. Shuwu, P. Liu, J. Ding, T. Jia, J. Qiu and Z. Sun, *Sci Rep*, 2015, **5,** 1337.
3 H. Dong, SR. Du, XY. Zheng, GM. Lyu, LD. Sun, LD. Li, PZ. Zhang, C. Zhang and CH. Yan, *Chem Rev*, 2015, **19**, 10725-815.
4 A. J. Amoroso and S. J. Pope, *Chem Soc Rev*, 2015, **44**, 4723-4742.
5 Z. Yi, W. Lu, Y. Xu, J. Yang, L. Deng, C. Qian, T. Zeng, H. Wang, L. Rao, H. Liu and S. Zeng, *Biomaterials*, 2014, **35**, 9689-9697.
6 L. Prodi, E. Rampazzo, F. Rastrelli, A. Speghini and N. Zaccheroni, *Chem Soc Rev*, 2015, **44**, 4922-4952.
7 M. Tsang, G. Bai and J. Hao *Chem Soc Rev*, 2015, **44**, 1585-1607.
8 A. H. Elmenoufy, Y. Tang, J. Hu, H. Xu and X. Yang, *Chem Commun*, 2015, **51**, 12247-12250.
9 H. Xing, S. Zhang, W. Bu, X. Zheng, L. Wang, Q. Xiao, D. Ni, J. Zhang, L. Zhou, W. Peng, K. Zhao, Y. Hua and J. Shi, *Adv Mater*, 2014, **26**, 3867-3872.
10 Y. Wu, Y. Sun, X. Zhu, Q. Liu, T. Cao, J. Peng, Y. Yang, W. Feng and F. Li, *Biomaterials*, 2014, **35**, 4699-4705.
11 T. Tegafaw, W. Xu, M. W. Ahmad, J. S. Baeck, Y. Chang, J. E. Bae, K. S. Chae, T. J. Kim and G. H. Lee, *Nanotechnology*, 2015, **26**, 0957-4484.
12 D. Ni, J. Zhang, W. Bu, H. Xing, F. Han, Q. Xiao, Z. Yao, F. Chen, Q. He, J. Liu, S. Zhang, W. Fan, L. Zhou, W. Peng and J. Shi, *ACS Nano*, 2014, **8**, 1231-1242.
13 Y. Sun, X. Zhu, J. Peng and F. Li, *ACS Nano*, 2013, **7**, 11290-11300.
14 V. Biju, M. Hamada, K. Ono, S. Sugino, T. Ohnishi, E. S. Shibu, S. Yamamura, M. Sawada, S. Nakanishi, Y. Shigeri and S. Wakida, *Nanoscale*, 2015, **7**, 14829-14837.
15 A. Xia, M. Chen, Y. Gao, D. Wu, W. Feng and F. Li, *Biomaterials*, 2012, **33**, 5394-5405.
16 X. Zhu, J. Zhou, M. Chen, M. Shi, W. Feng and F. Li, *Biomaterials*, 2012, **33**, 4618-4627.
17 H. Xing, W. Bu, S. Zhang, X. Zheng, M. Li, F. Chen, Q. He, L. Zhou, W. Peng, Y. Hua and J. Shi, *Biomaterials*, 2012, **33**, 1079-1089.
18 M. Kidoh, D. Utsunomiya, S. Oda, Y. Funama, H. Yuki, T. Nakaura, N. Kai, T. Nozaki and Y. Yamashita, *Int J Cardiovasc Imaging*, 2015, **6**, 6.
19 O. A. Catalano, M. S. Gee, E. Nicolai, F. Selvaggi, G. Pellino, A. Cuocolo, A. Luongo, M. Catalano, B. R. Rosen, D. Gervais, M. G. Vangel, A. Soricelli and M. Salvatore, *Radiology*, 2015, **5**, 150566.
20 A. J. Shuhendler, D. Ye, K. D. Brewer, M. Bazalova-Carter, K. H. Lee, P. Kempen, K. Dane Wittrup, E. E. Graves, B. Rutt and J. Rao, *Sci Rep*, 2015, **5**.
21 G. H. Gundersen, T. M. Norekval, H. H. Haug, K. Skjetne, J. O. Kleinau, T. Graven and H. Dalen, *Heart*, 2015, **5**, 2015-307798.
22 Y. Han, S. Tzoumas, A. Nunes, V. Ntziachristos and A. Rosenthal, *Med Phys*, 2015, **42**, 4928596.
23 Z. Liu, F. Pu, J. Liu, L. Jiang, Q. Yuan, Z. Li, J. Ren and X. Qu, *Nanoscale*, 2013, **5**, 4252-4261.
24 F. Li, C. Li, J. Liu, X. Liu, L. Zhao, T. Bai, Q. Yuan, X. Kong, Y. Han, Z. Shi and S. Feng, *Nanoscale*, 2013, **5**, 6950-6959.
25 K. Ai, Y. Liu, J. Liu, Q. Yuan, Y. He and L. Lu, *Adv Mater*, 2011, **23**, 4886-4891.
26 Y. Liu, K. Ai, J. Liu, Q. Yuan, Y. He and L. Lu, *Angew Chem Int Ed Engl*, 2012, **51**, 1437-1442.
27 Y. Wang, S. Song, J. Liu, D. Liu and H. Zhang, *Angew Chem Int Ed Engl*, 2015, **54**, 536-540.
28 L. Zhou, X. Zheng, Z. Gu, W. Yin, X. Zhang, L. Ruan, Y. Yang, Z. Hu and Y. Zhao, *Biomaterials*, 2014, **35**, 7666-7678.
29 H. Zhang, H. Wu, J. Wang, Y. Yang, D. Wu, Y. Zhang, Z. Zhou and S. Yang, *Biomaterials*, 2015, **42**, 66-77.
30 S. Dharmadhikari, J. R. James, J. Nyenhuis and N. Bansal, *Magn Reson Med*, 2015, **15**, DOI: 10.1002/mrm.25792.
31 G. Rancan, D. Delli Castelli and S. Aime, *Magn Reson Med*, 2016, **1**, 329-336.
32 L. Zhang, L. Zeng, Y. Pan, S. Luo, W. Ren, A. Gong, X. Ma, H. Liang, G. Lu and A. Wu, *Biomaterials*, 2015, **44**, 82-90.

33 J. Li, J. You, Y. Dai, M. Shi, C. Han and K. Xu, *Anal Chem*, 2014, **86**, 11306-11311.
34 G. Tian, X. Zheng, X. Zhang, W. Yin, J. Yu, D. Wang, Z. Zhang, X. Yang, Z. Gu and Y. Zhao, *Biomaterials*, 2015, **40**, 107-116.
35 P. Qiu, R. Sun, G. Gao, C. Zhang, B. Chen, N. Yan, T. Yin, Y. Liu, J. Zhang, Y. Yang and D. Cui, *Theranostics*, 2015, **5**, 456-468.
36 S. Lu, D. Tu, P. Hu, J. Xu, R. Li, M. Wang, Z. Chen, M. Huang and X. Chen, *Angew Chem Int Ed Engl*, 2015, **54**, 7915-7919.
37 R. Weissleder and M. J. Pittet, *Nature*, 2008, **452**, 580-589.
38 Y. Wu, M. Shi, L. Zhao, W. Feng, F. Li and C. Huang, *Biomaterials*, 2014, **35**, 5830-5839.
39 S. Zeng, H. Wang, W. Lu, Z. Yi, L. Rao, H. Liu and J. Hao, *Biomaterials*, 2014, **35**, 2934-2941.
40 C. Li, P. A. Ma, P. Yang, Z. Xu, G. Li, D. Yang, C. Peng and J. Lin, *CrystEngComm*, 2011, **13**, 1003-1013.
41 Q. Zeng, B. Xue, Y. Zhang, D. Wang, X. Liu, L. Tu, H. Zhao, X. Kong and H. Zhang, *CrystEngComm*, 2013, **15**, 4765-4772.
42 R. Lv, G. Yang, Y. Dai, S. Gai, F. He and P. Yang, *CrystEngComm*, 2014, **16**, 9612-9621.
43 Y. Liu, D. Tu, H. Zhu and X. Chen, *Chem Soc Rev*, 2013, **42**, 6924-6958.

Table of Contents

Core-shell $BaYbF_5$:Tm@$BaGdF_5$:Yb,Tm nanocrystals for in vivo tri-modal UCL/CT/MR imaging

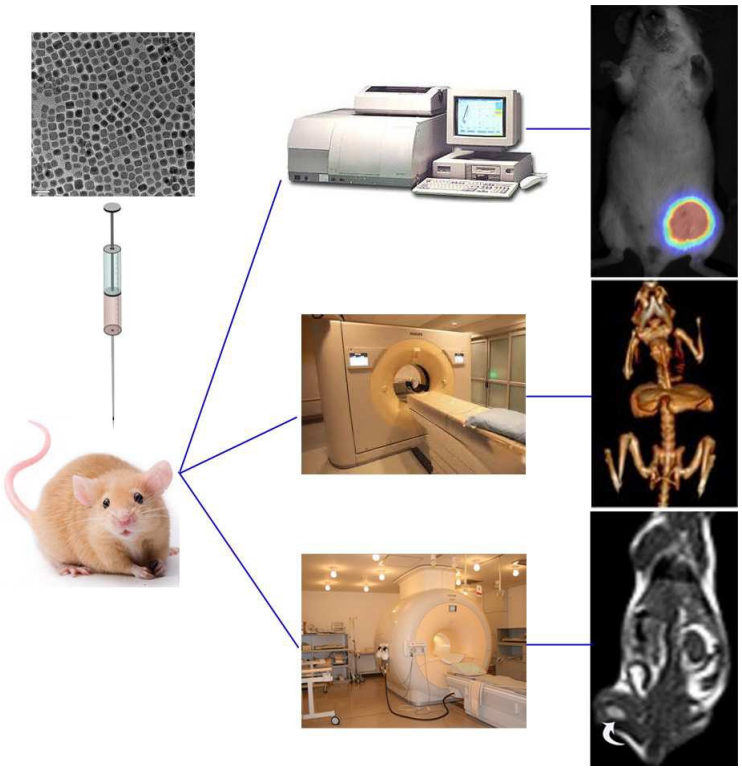

A PEGylated Core-shell $BaYbF_5$:Tm@$BaGdF_5$:Yb,Tm nanocrystals have been constructed and successfully applied as the UCL imaging, CT imaging and MR imaging.